LiCoO2 with double porous structure obtained by electrospray deposition and its evaluation as an electrode for lithium-ion batteries

Ilham Bezza, Erwann Luais, Fouad Ghamouss, Mustapha Zaghrioui, François Tran-Van, Joe Sakai

LiCoO2 with double porous structure obtained by electrospray deposition and its evaluation as an electrode for Lithium-ion batteries

Ilham Bezza,[1] Erwann Luais,[1,2] Fouad Ghamouss,[1,*] Mustapha Zaghrioui,[2] François Tran-van,[1] Joe Sakai[2]

[1] PCM2E, EA 6299 Université François Rabelais de Tours, Parc de Grandmont 37200 Tours, France

[2] GREMAN, UMR 7347 CNRS/Université François Rabelais de Tours, Parc de Grandmont 37200 Tours, France

* Corresponding author: ghamouss@univ-tours.fr

Abstract

An *in-situ* temperature-controlled Raman spectroscopy aided unique electrode fabrication technique has been developed for Li-ion battery applications, ensuring superior electrochemical quality of the multi-porous $LiCoO_2$ films with higher stoichiometric purity of high temperature (HT)-$LiCoO_2$ phase, by observing the structural changes during the fabrication process and thus confirming the transformation from the low temperature (LT)-$LiCoO_2$ phase. This much desired simple process is not only free of any sort of binders or carbon additives but also works at atmospheric pressure, leading to a very simple deposition technique using a homemade and inexpensive set-up. Also, the time of depositions were varied and resultant films we investigated for their electrochemical performance. The high-resolution scanning electron microscope (SEM) observation has revealed not only a µm-size porous structure but also three-dimensional cross-link with 10 nm-level pores of the material, which ensured the much-desired porosity for high-performance cathodes.

Keywords: Li-ion batteries, cathode, electrostatic spray deposition, HT-$LiCoO_2$, porous layer, specific capacity.

1. Introduction

Lithium-ion battery (LIB) production continues to grow as the demand of the electronics industry, especially for mobile phones and computers, increases. Therefore, active research continues on all aspects of batteries, including anode and cathode elaboration, new electrolytes, cells assembly, interface studies and so on.

Lithium cobalt oxide, $LiCoO_2$, was first proposed by Goodenough's group and used for the first time as a thin film cathode in 1980 [1] and it's still considered in many applications including microdevices, e.g. smart labels, active radiofrequency identification (RFID), smarts cards, biomedical applications, and wireless [2–4]. Even though that this cathode material is a long-established conventional material, intense researches are still ongoing aiming the development of efficient $LiCoO_2$ material with suitable morphology and structure [5,6]. In this context, several physical deposition techniques have been implemented by several groups including Physical Vapor Deposition (PVD), Atomic Layer Deposition (ALD) and so on [2,7–10]. However, most of these techniques are onerous and time-consuming. These deposition methods also lead, in general, to very dense films excluding the bulk of the film from the contribution to the storage reaction. Indeed, poor Li^+ diffusion can be observed if the electrode morphology is too dense with not enough porosity for ion transportation. Lots of research efforts have been put to address this issue, different nanostructures with high surface area, such as nanowires, mesoporous sponges, core-shell structures, and nanoplates have been synthesized to obtain short effective diffusion length for Li^+, in order to improve reaction kinetics. With this, a well-established porous network is indeed required to enable faster ion diffusions within the bulk of the electrode to finally enable high rate performance [11–13]. In addition, a well-formed nano-porosity helps to accommodatethe expanded volume of the active materials during lithiation and hence enhances the stability of the electrode, also sufficient porosity helps increasing contact areas between the electrode material and electrolyte ions, which enhances electrochemical performances. Therefore, alternative deposition methods have to be implanted to overcome such issues and providing materials with low cost, controlled morphology and structure.

In this work, we report our simple electrode fabrication process by electrostatic spray deposition (ESD) technique to deposit high quality porous $LiCoO_2$ films. The electrostatic spray deposition (ESD) is a technique that has been developed to fabricate inorganic and porous films. Its basic principle is the generation of an aerosol using a mixture of organic solvents and inorganic precursors under an applied high voltage. The precursor liquid is pumped through a nuzzle to form spherical shape at its tip which is transformed into a conical

shape at applied high voltage. The charged droplets formed aerosol is sequentially deposited on a heated substrate to construct the desired thin film [14–17].

ESD allowed electrodes to be synthesized without any additives, such as polymer binders, conductive additives (e.g. carbon black), etc. This not only enhances the purity of the as-prepared films but also ensures the presence of no dead volume of the active material within the electrode. In addition, ESD is well known to form a porous network within the formed film with constituent particles (sprayed), for fast electrolyte diffusion and for the accommodation of the volume variation during the charge and the discharge of the electrode. ESD ensures excellent cohesive attachment of the constituent particles (sprayed) [18] and hence removes the uncertainties involved with possible breakage of the conduction bridges formed by the conductive additives, and hence ensures no fluctuations in the internal resistance of the cathodes.

We carried out the entire deposition process at the air atmosphere and hence we used the simplest homemade set-up, and ESD allowed us to control several deposition parameters very easily. We controlled the rate of deposition and temperature of the fabrication process, and hence the thickness and quality of the films. The process was optimized to achieve high-purity material and optimal electrochemical performance. To ensure the quality of as-prepared films, *in situ* temperature-controlled micro-Raman spectroscopy was carried out during the fabrication process, and evaluation of phases of $LiCoO_2$ was monitored. The formation of HT-phase $LiCoO_2$ during annealing was confirmed, which ensured enhanced electrochemical performances. The resulting porous structure was characterized by optical images and high-resolution scanning electron microscopy (SEM), followed by electrochemical characterization.

2. Experimental

2.1 Synthesis method

Precursor solutions were made from lithium acetate dihydrate; [Li $(CH_3COO)_2$, $2H_2O$] and cobalt acetate tetrahydrate; [$Co(CH_3COO)_2$, $2H_2O$] dissolved into the mixture of ethanol (C_2H_5OH) and butyl carbitol [$CH_3(CH_2)_3(OCH_2CH_2)_2OH$] (molar ratio 1:1). Four types of precursors with different Li/Co ratios such as 1:1, 1.05:1, 1.1:1, and 1.2:1 were prepared. The precursor solutions were stirred magnetically for 24 hours to be homogenized.

The setup of the ESD used in this work is shown in Figure 1. A stainless-steel (SS) nozzle (2 mm in inner diameter), connected through a silicone tube to a syringe that supplies the precursor solution with the help of a syringe pump, is electrically connected to a high voltage source, whereas the substrate heater is grounded. During the deposition, the nozzle is biased

to a high voltage to generate a high electrostatic force that atomizes the liquid at the tip of the nozzle and accelerates the charged droplets forming an aerosol that is sequentially deposited on a heated substrate (50 µm-thick SS foil) to form the desired film. The nozzle voltage and the substrate temperature were set at +8 kV and 250˚C, respectively, while the flow rate of the precursor was varied from 0.2 to 0.7 ml/h.

The obtained films were annealed in the air for 2 hours at different temperatures from 100°C to 650°C. The heating and cooling rate was 1°C/min.

[Figure 1 about here]

2.2 Structural characterizations

In order to monitor the phase changes during heating, *in situ* temperature-controlled micro-Raman spectroscopy was performed using a reflex device (Renishaw, inVia). A laser with 632.8 nm in wavelength and 1 mW in power and a x50 objective lens were used as the excitation light source. A commercial temperature control stage (Linkam, THMS 600) was used to anneal the as-deposited film from the room temperature to 600°C in air. The microstructure of the deposited layers was observed using the scanning electron microscopy (SEM; Zeiss, ULTRA Plus).

2.3 Electrochemical tests

Half-cells were assembled in an Ar-filled glovebox (O_2 level < 2 ppm) as the form of coin cells of type 2032, each of which contained a lithium foil and as prepared $LiCoO_2$ thick film as the reference and working electrodes respectively, separated by a polypropylene membrane (Celgard, 2400). The liquid electrolyte used in the half-cells is a mixture of ethylene carbonate (EC), propylene carbonate (PC) and dimethyl carbonate (DMC), and lithium hexafluorophosphate ($LiPF_6$) as the electrolytic salt. The mass ratio of EC/PC/DMC is 1: 1: 3. Electrochemical measurements including galvanostatic cycling and cyclic voltammetry (CV) were performed with a multi-channel potentiostat (Biologic, VMP3). Galvanostatic charge-discharge cycling tests were performed on the samples annealed at different temperatures under constant current conditions and voltage limitation. Current rates from 50 to 300 µA/cm^2 were applied to investigate the rate capability of the prepared materials. Cyclic voltammetry (CV) was performed starting from the open circuit voltage (around 3 V) to 4.2 V at a scan rate of 0.05 mV/s.

3. Results and discussion

3.1 Structural characterizations

The quality of $LiCoO_2$ film strongly depends upon the type of the crystallinity of $LiCoO_2$ materials, as they have two different phases, which are very different in nature and hence they significantly control the electrochemical properties of the electrodes. The first structure, a rhombohedral structure that belongs to the space group R3m is generally obtained at high temperature (HT) is a very ordered lamellar structure. This structure is commonly referred to as high-temperature (HT)-$LiCoO_2$ phase and this is the structure of choice because of its superior cycle stability, reversibility.

The second structure, i.e., the so-called low-temperature (LT)-$LiCoO_2$, crystallizes at approximately 400°C in a spinel-like structure that belongs to the space group Fd3m [19]. As this structure lacks an ordered morphology, intercalation of Li is not as good as in the case of HT- LiCoO2 cathodes which exhibit high specific capacity with high reversibility thanks to its well defined layered structure. The layered structure promotes an easier exchange of Li^+ ions, thanks to the interlayer spaces which acts as well-defined channels for easier interlayer ion diffusions.

Therefore, it's very important to obtain HT-$LiCoO_2$ to get high-quality cathodes, which can be ensured at its best when monitored in-situ during the electrode fabrication.

In order to determine the effect of the annealing temperature, Raman spectra of the as-deposited sample were recorded in situ during the heating process in the air between room temperature and 600°C. Different spectra obtained at selected temperatures are shown in Figure 2. The Raman patterns at a temperature above 600°C were not presented due to the oxidation of the substrate.

Raman spectrum of the as-deposited film (spectrum at 26 °C in Figure 2) consists of a non-lithiated cobalt oxide Co_3O_4, whose representative bands are approximately at 195, 483, 529, 622 and 689 cm^{-1}, which are attributed to F_{2g}, E_g, F_{2g}, F_{2g} and A_{1g} Raman modes, respectively [20,21]. With increasing temperature, a first phase change occurs at a temperature above 350°C. Indeed, between 350 and 400 °C, we observed the disappearance of the band at 195 cm^{-1}, suggesting the disappearance of the Co_3O_4 phase. Raman signals located around 445, 476, 580 and 676 cm^{-1} are attributed to E_g, F_{2g}, F_{2g} and A_{1g} modes, respectively, of LT-$LiCoO_2$[16–18]. The second phase change occurs above 500 °C and the obtained spectra are characteristic of the $LiCoO_2$ high-temperature phase (HT-$LiCoO_2$) [22–24]. The bands located approximately at 472 and 585 cm^{-1} are assigned to E_g and A_{1g} phonon modes.

The annealing parameters of the layers that we synthesize by ESD are usually 2 hours and a temperature of 600 °C where a pure high-temperature phase of $LiCoO_2$ was obtained. However, results of Figure 2 suggest that HT-$LiCoO_2$ phase can be also obtained at relatively

low temperature (500 ˚C). This temperature is lower than those used in previous reports [19], thanks to the possible control over the slow rate of heating of the sample and monitoring the phases by in-situ temperature controlled Raman analysis. Moreover, this finding may widen the choice of substrate materials to non-durable substrate against high temperatures.

[Figure 2 about here]

Raman spectra for four samples prepared from precursors with different Co/Li ratio and annealed at 600°C are shown in Figure S1, which may provide a qualitative study on the effect of the different Co/Li ratios on the obtained HT-$LiCoO_2$. These spectra clearly show the formation of HT-$LiCoO_2$ phase as evidenced by the presence of the Raman modes at 486 cm^{-1} and 595 cm^{-1}. However, the presence of Co_3O_4 phase (mode at about 195 cm^{-1}) is detected in samples obtained from a precursor with Co/Li ratio of 1. The presence of Co_3O_4 impurity could indicate partial evaporation of Li during the deposition and/or annealing. Meanwhile, this impurity is not visible for the other samples with Co/Li of 0.95, 0.91 and 0.83. Therefore, we can reasonably conclude that the precursor is required to be Li-rich with at least 0.91 of Co/Li ratio in order to ensure maximum conversion of formed Co_3O_4 into $LiCoO_2$ and hence avoiding any impurity in the film from residual Co_3O_4.

Figures 2S(**a-d**) show optical microscope images of four HT-$LiCoO_2$ films. These images clearly highlight the porous morphology of the obtained films. Moreover, the sizes of the pores of these four films are clearly different. Since these films are obtained using a different flow rate of the precursors (0.2, 0.3, 0.4 and 0.5mL/h), we can reasonably conclude that pores size may be controlled by controlling this parameter.

The evolution of the pore diameter determined from the observation of different optical microscope images is illustrated in table 1, and it was observed that the pore diameter was increased when the flow rate of the precursor solution was increased.

[Table 1 about here]

Figure 3a summarizes the relationship between the pore size of $LiCoO_2$ films and the flow rate of the precursor during deposition. Two zones are observed: porous zone obtained at flow rates under 0.5 mL/h and above this value a dense zone where we could not see any pores.

The effect of these two morphologies on the electrochemical test is illustrated in Figure 3b. The electrochemical behavior of the porous and the dense films are identical to the $LiCoO_2$ material described in the literature [25–27]. However, the dense film shows two broad redox signals which must be caused by the poor lithium diffusion on the structure. For the porous film, the faradic current is higher than that of the dense film, this may imply that the porous film has a higher capacity, due to the larger active surface. Therefore, the lithium insertion or extraction in a $LiCoO_2$ layer is found to be strongly dependent on the morphology of the film.

[Figure 3 about here]

Figures 4**(a-f)** show SEM images, before and after the annealing at 600 °C for 2 hours, of a $LiCoO_2$ film deposited on a Stainless Steel (SS) substrate at 250°C with a flow rate of 0.3 mL/h and a precursor ratio, Co/Li of 0.91. As can be seen in Figures 4**(a-c)**, the $LiCoO_2$ before annealing had a three-dimensional porous network structure with uniformly monodispersed circular pores. The material is fibrous, with relatively smooth surface indicating its amorphous nature. Before annealing, the size of the pores is in the range of 2 – 4 µm. After annealing (Figure 4**(d-f)**), the surface structures of the sample become more 3D-like and the thickness of the walls between the pores is thinner. These could be due to the evaporation of some organic component in the deposited amorphous film and to its crystallization. On the other hand, SEM images obtained at higher magnification showed that the walls of these pores are themselves porous. This could be due to the nanocrystals which formed the walls, apparently originating in the fibers that existed in the as-deposited film. The nanocrystal size is around 50 nm. Such double-porous structure, realizing huge surface area, may be advantageous for the material wetting by the electrolyte, the diffusion of Li^+, and for the charge transfer during the electrochemical process involved with the charge and discharge process of batteries.

[Figure 4 about here]

The following tests were performed on the $LiCoO_2$ films prepared from a precursor of Co/Li = 0.91 corresponded to $Li_{1.1}CoO_2$, with a flow rate of 0,5 mL/h and the post annealing at 600°C for 2h.

3.2 Electrochemical tests

CV curves of $LiCoO_2$ films annealed at three temperatures (at 550°C, 575°C and 600°C for 2 h) were recorded with the scan rate of 0.05 mVs^{-1} and compared in Figure 5. The depicted curves show a difference of 50 mA/g in the maximum current intensity between the film annealed at 600°C and the two films annealed at 550°C and 575°C. This difference is obviously due to the enhanced capacity obtained for the film annealed at a higher temperature. The CV profiles are almost the same for the three samples. During the anodic sweep, lithium ions are extracted from the $LiCoO_2$ cathode and oxidation current is observed. Four oxidation peaks are observed at 3.84, 4.00, 4.10 and 4.19 V during the forward sweep and four reduction peaks at 3.81, 3.86, 4.05 and 4.15 V during the reverse sweep, indicating the reversibility of the electrochemical reaction

The obvious redox peak centered at (**4.00 V/3.86 V**) is attributed to the deintercalation and intercalation reactions of Li^+ ions in HT-$LiCoO_2$, whereas the small anodic peak around 3.84 V corresponds to deintercalation reaction of a less-crystallized phase. However, and according to the Raman results, this phase would not be an LT-$LiCoO_2$ phase. Above 4V, there are two small redox peaks (**4.10V/4.05V**) and (**4.19V/4.15V**), which are caused by the order-disorder phase transition. The CV curves show a slight separation between the peaks of lithium insertion (reduction) and extraction (oxidation). This is probably due to the electrolyte and electrode resistivity causing an ohmic drop during the current flow.

[Figure 5 about here]

Galvanostatic cycling with potential limitation was also performed and the effect of the annealing temperature on the specific capacity was studied. Figure S3 depicts the discharge capacity of $LiCoO_2$ cathodes prepared by ESD with the flow rate of 0.5 mL/h and Co/Li of 0.91 and annealed at different temperatures: 550°C, 575°C, 600°C, 625°C, and 650°C. As shown in this figure, the $LiCoO_2$ layer annealed at 600°C exhibits the highest capacity. The electrode exhibits a capacity of 179.6 µAh/cm² at a discharge current of 50 µA/cm². A slight decrease of the capacity is observed by increasing the discharge current. However, the capacity fading is reasonable, and the electrode still exhibits around 89 % of its initial capacity at a discharge current of 300 $\mu A/cm^2$. Samples annealed at 550°C and 575 °C showed lower capacity, 150 and 154 $\mu Ah/cm^2$ at a discharge current of 50$\mu A/cm^2$. For these two samples, the rate of the capacity fading under higher discharge current is almost similar and close to samples annealed at 600°C. However, annealing the samples at 625°C and 650

°C leads to relatively lower capacity. Indeed, only 127 µAh/cm^2 at 50 µA/cm^2 is reached by the sample annealed at 625°C and the capacity fading is more prominent when the discharge current is increased. This behavior is even more marked with higher annealing temperature (650°C). Such a high annealing temperature definitely deteriorates the electrochemical performance of the materials. Assuming that the porous structure is mainly controlled by the flow rate during the ESD process and that high annealing temperature leads to defined phase and purer HT-$LiCoO_2$, the relatively low capacity observed in samples annealed at 625°C and 650°C might be due to the oxidation of the SS substrate. Oxidation of the substrate can increase the resistivity of the electrode and the contact resistance between $LiCoO_2$ and the substrate. Moreover, interdiffusion between the stainless substrate and LiCoO2 may be also possible with the increase of annealing temperature.

The effect of the mass of the deposited film was also examined. Figure 4S**a** shows the evolution of C/C_0 of HT-$LiCoO_2$ films deposited for a different time as functions of C-rate. As expected, increasing the deposition time is accompanied by lowering the gravimetric capacities of discharge. Such a result could be explained by the increase of the diffusion path of Li ions and the electrical resistivity of the sample. This is well evidenced by the fact that the specific capacitance is almost the same at a low discharge rate (allowing enough time for the diffusion of species into the materials). In addition, the contribution of the resistivity of the material is well evidenced by the drastic fading of the specific capacity, especially in the case of deposition time of 180 min. For this last, the C/Co is almost negligible which can be justified by slow diffusion through the thick film. In Figure 4S**b**, the gravimetric capacity at a current rate of 1C is plotted as a function of deposition time, showing a slight decrease of around 8%. The surface capacity increases almost linearly according to the deposition time (right axis of Figure 4S**b**), with an only slight deviation from the straight line, indicating that the electrochemical activity is almost independent of the thickness in the range of studied thickness and for the rate 1C. We can conclude that even with the dense film we will not lose a lot of gravimetric capacity.

The specific capacity under different current densities (from 50 to 300 µAh/cm^2), as well as the retention during long cycling, is shown in Figures 6**a** and 6**b**. We note that the capacity after 100 cycles was 85% of the initial value, which indicates an excellent retention property of the material. One reason for this very good stability and good retention at high current would be the absence of binder and the high surface area. The porosity is advantageous to the penetration of the electrolyte and to the adaption of the volume changes of $LiCoO_2$ during the charge-discharge process. Moreover, thanks to the absence of the binder in this cathode

material, the electrolyte will be able to access easily to the surface of the material, which facilitates the diffusion of Li^+ ions in $LiCoO_2$ framework, which d significantly reduces the polarization during charge-discharge process.

[Figure 6 about here]

4. Conclusion

We had demonstrated a very simple fabrication technique and obtained high quality porous $LiCoO_2$ films on stainless steel substrates by the ESD technique with the precursor based on Li and Co acetates. An *In-situ* temperature-controlled Raman analysis confirmed the gradual transformation from LT- to HT-$LiCoO_2$ phase in a temperature region of 450 – 550˚C. This *in-situ* observation was the key to ensure maximum conversion of formed Co_3O_4 into $LiCoO_2$, and we successfully demonstrated the importance of Li-rich precursors, determining a Co/Li ratio; required to make the resulting films free from Co_3O_4 impurity. High-resolution SEM observation revealed that the typical $LiCoO_2$ films showed double porous structure, consisting of µm-sized pores whose diameter depends on the flow rate of the precursor and nm-level pores originating in fibrous structure in the as-deposited film. Cycling test showed that the $LiCoO_2$ film deposited by the ESD method and annealed at 600°C shows good cycling characteristics at the different current rate. This synthesis method could also be used to prepare other oxide materials either for anode such as $Li_4Ti_5O_{12}$ and for cathode such as $LiMn_{0.5}Ni_{0.5}O_2$

Acknowledgment

This study was supported by Région Centre, France, through the BLaDES and µBaGS projects, and by the French Government through the Investissements d'Avenir Tours2015 project. Authors thank Dr. Arunabh Ghosh for his valuable help which significantly enriched the article.

References

[1] K. Mizushima, P.C. Jones, P.J. Wiseman, J.B. Goodenough, Li_xCoO_2 (0< x<-1): A new cathode material for batteries of high energy density, Mater. Res. Bull. 15 (1980) 783–789.

[2] E.M.F. Vieira, J.F. Ribeiro, M.M. Silva, L. Dupont, J.H. Correia, L.M. Goncalves, Flexible solid-state Li–ion battery using ge thin film anode and $LiCoO_2$ cathode, in: 26th Micromechanics Microsystems Eur. Conf., 2015.

[3] H. Xia, Y. Wan, W. Assenmacher, W. Mader, G. Yuan, L. Lu, Facile synthesis of chain-like $LiCoO_2$ nanowire arrays as three-dimensional cathode for microbatteries, NPG Asia Mater. 6 (2014) e126.

[4] R. Hahn, M. Ferch, N.A. Kyerematen, K. Hoeppner, K. Marquardt, G.A. Elia, Characteristics of Li-ion micro batteries fully batch fabricated by micro-fluidic MEMS packaging, Microsyst. Technol. (2018). doi:10.1007/s00542-018-3933-z.

[5] B. Wu, J. Wang, J. Li, W. Lin, H. Hu, F. Wang, S. Zhao, C. Gan, J. Zhao, Morphology controllable synthesis and electrochemical performance of $LiCoO_2$ for lithium-ion batteries, Electrochim. Acta. 209 (2016) 315–322.

[6] L. Huang, R.M. Mank, Y. Chen, Method to improve $LiCoO_2$ morphology in thin film batteries, (2018).

[7] M.E. Donders, W.M. Arnoldbik, H.C.M. Knoops, W.M.M. Kessels, P.H.L. Notten, Atomic layer deposition of LiCoO2 thin-film electrodes for all-solid-state Li-ion micro-batteries, J. Electrochem. Soc. 160 (2013) A3066–A3071.

[8] J. Xie, J. Zhao, Y. Liu, H. Wang, C. Liu, T. Wu, P.-C. Hsu, D. Lin, Y. Jin, Y. Cui, Engineering the surface of $LiCoO_2$ electrodes using atomic layer deposition for stable high-voltage lithium ion batteries, Nano Res. 10 (2017) 3754–3764.

[9] M. Yoon, S. Lee, D. Lee, J. Kim, J. Moon, All-solid-state thin film battery based on well-aligned slanted $LiCoO_2$ nanowires fabricated by glancing angle deposition, Appl. Surf. Sci. 412 (2017) 537–544.

[10] H. Zhang, R.E. Demaray, Deposition of $LiCoO_2$, (2018).

[11] S. Kazemiabnavi, R. Malik, B. Orvananos, A. Abdellahi, G. Ceder, K. Thornton, The effect of surface-bulk potential difference on the kinetics of intercalation in core-shell active cathode particles, J. Power Sources. 382 (2018) 30–37.

[12] F. Jiao, K.M. Shaju, P.G. Bruce, Synthesis of Nanowire and Mesoporous Low-Temperature $LiCoO_2$ by a Post-Templating Reaction, Angew. Chemie Int. Ed. 44 (2005) 6550–6553.

[13] L. Hu, J.W. Freeland, J. Cabana, Surface Chemistry, Passivation and Electrode Performance in Core-Shell Architectures of $LiCoO_2$ Nanoplates, ACS Appl. Energy Mater. (2019).

[14] C.H. Chen, E.M. Kelder, M.J.G. Jak, J. Schoonman, Electrostatic spray deposition of thin layers of cathode materials for lithium battery, Solid State Ionics. 86 (1996) 1301–1306.

[15] C.H. Chen, E.M. Kelder, J. Schoonman, Unique porous $LiCoO_2$ thin layers prepared by electrostatic spray deposition, J. Mater. Sci. 31 (1996) 5437–5442.

[16] S. Leeuwenburgh, J. Wolke, J. Schoonman, J. Jansen, Electrostatic spray deposition (ESD) of calcium phosphate coatings, J. Biomed. Mater. Res. Part A. 66 (2003) 330–334.

[17] X.-H. Ma, Q.-Y. Wan, X. Huang, C.-X. Ding, Y. Jin, Y.-B. Guan, C.-H. Chen, Synthesis of three-dimensionally porous MnO thin films for lithium-ion batteries by improved Electrostatic Spray Deposition technique, Electrochim. Acta. 121 (2014) 15–20.

[18] Y.-N. Zhou, M.-Z. Xue, Z.-W. Fu, Nanostructured thin film electrodes for lithium storage and all-solid-state thin-film lithium batteries, J. Power Sources. 234 (2013) 310–332.

[19] S.G. Kang, S.Y. Kang, K.S. Ryu, S.H. Chang, Electrochemical and structural properties of HT-$LiCoO_2$ and LT-$LiCoO_2$ prepared by the citrate sol-gel method, Solid State Ionics. 120 (1999) 155–161.

[20] S. Xiong, C. Yuan, X. Zhang, B. Xi, Y. Qian, Controllable synthesis of mesoporous Co_3O_4 nanostructures with tunable morphology for application in supercapacitors, Chem. Eur. J. 15 (2009) 5320–5326.

[21] F. Giovannelli, V. Marsteau, M. Zaghrioui, C. Autret, F. Delorme, Low temperature synthesis of Co_3O_4 and $(Co_{1-x}Mn_x)_3O_4$ spinels nanoparticles, Adv. Powder Technol. 28 (2017) 1325–1331.

[22] C. Julien, Local cationic environment in lithium nickel–cobalt oxides used as cathode materials for lithium batteries, Solid State Ionics. 136 (2000) 887–896.

[23] C.M. Burba, K.M. Shaju, P.G. Bruce, R. Frech, Infrared and Raman spectroscopy of nanostructured LT-$LiCoO_2$ cathodes for Li-ion rechargeable batteries, Vib. Spectrosc. 51 (2009) 248–250.

[24] W. Huang, R. Frech, Vibrational spectroscopic and electrochemical studies of the low and high temperature phases of $LiCo_{1-x}M_xO_2$ (M= Ni or Ti), Solid State Ionics. 86 (1996) 395–400.

[25] L. Xue, S. V Savilov, V. V Lunin, H. Xia, Self-Standing Porous $LiCoO_2$ Nanosheet Arrays as 3D Cathodes for Flexible Li-Ion Batteries, Adv. Funct. Mater. 28 (2018) 1705836.

[26] Y.H. Rho, K. Kanamura, M. Fujisaki, J. Hamagami, S. Suda, T. Umegaki, Preparation of $Li_4Ti_5O_{12}$ and $LiCoO_2$ thin film electrodes from precursors obtained by sol–gel method, Solid State Ionics. 151 (2002) 151–157.

[27] I. Uchida, H. Sato, Preparation of Binder-Free, Thin Film $LiCoO_2$ and Its Electrochemical Responses in a Propylene Carbonate Solution, J. Electrochem. Soc. 142 (1995) L139–L141.

Figures list

Table list

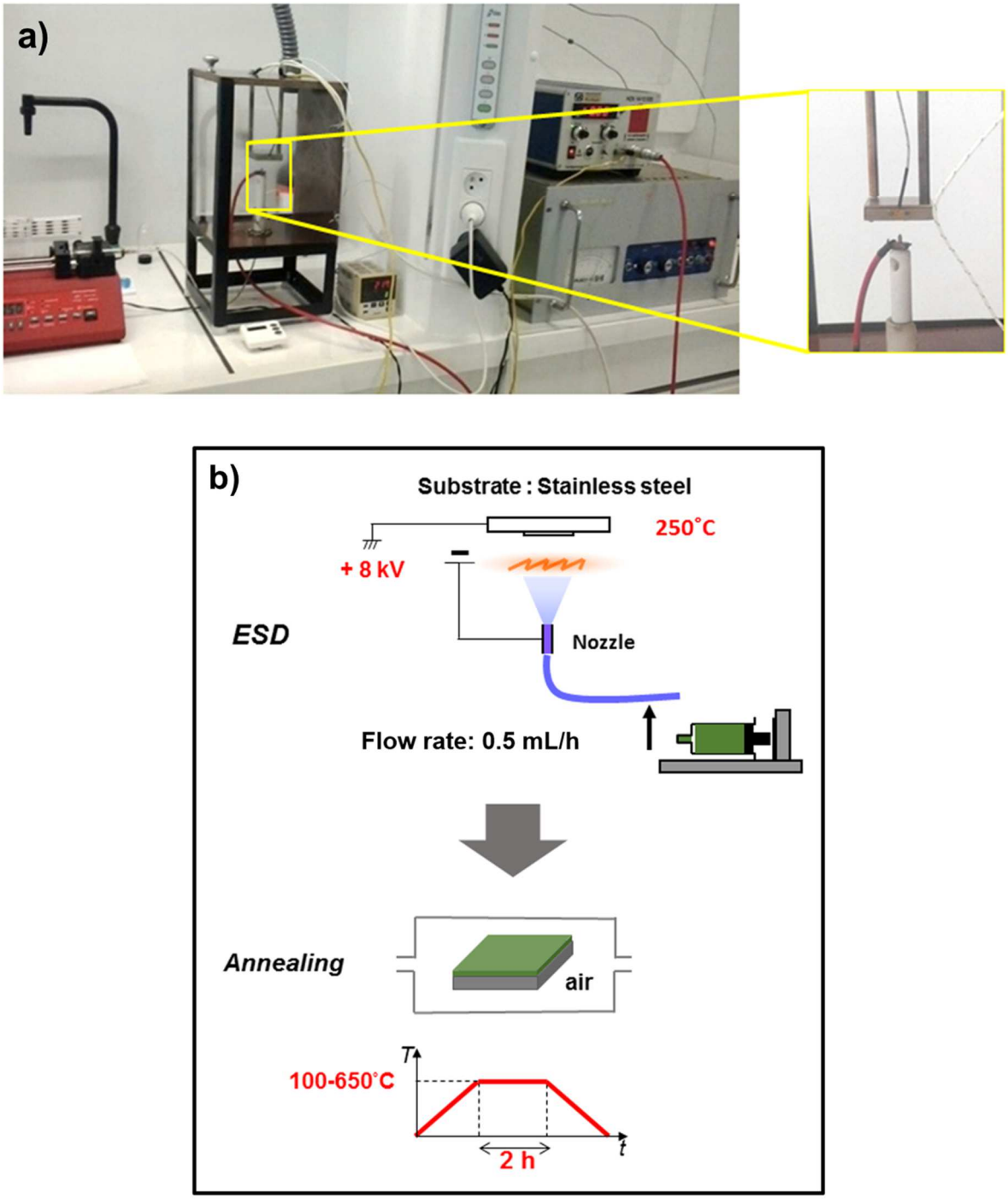

Figure 1: (a) ESD experimental set-up, (b) schematic of the ESD process

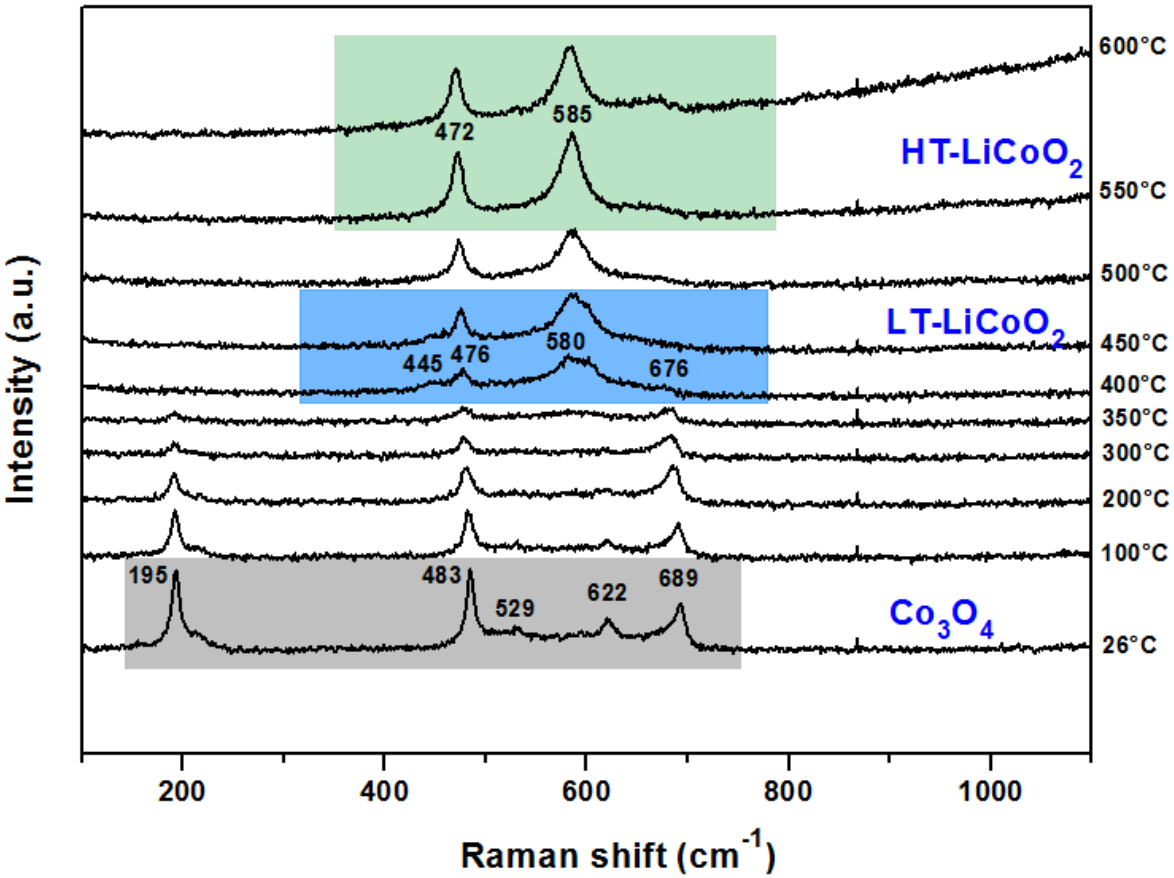

Figure 2: *In situ* temperature-controlled micro-Raman spectra of a $LiCoO_2$ film during heating.

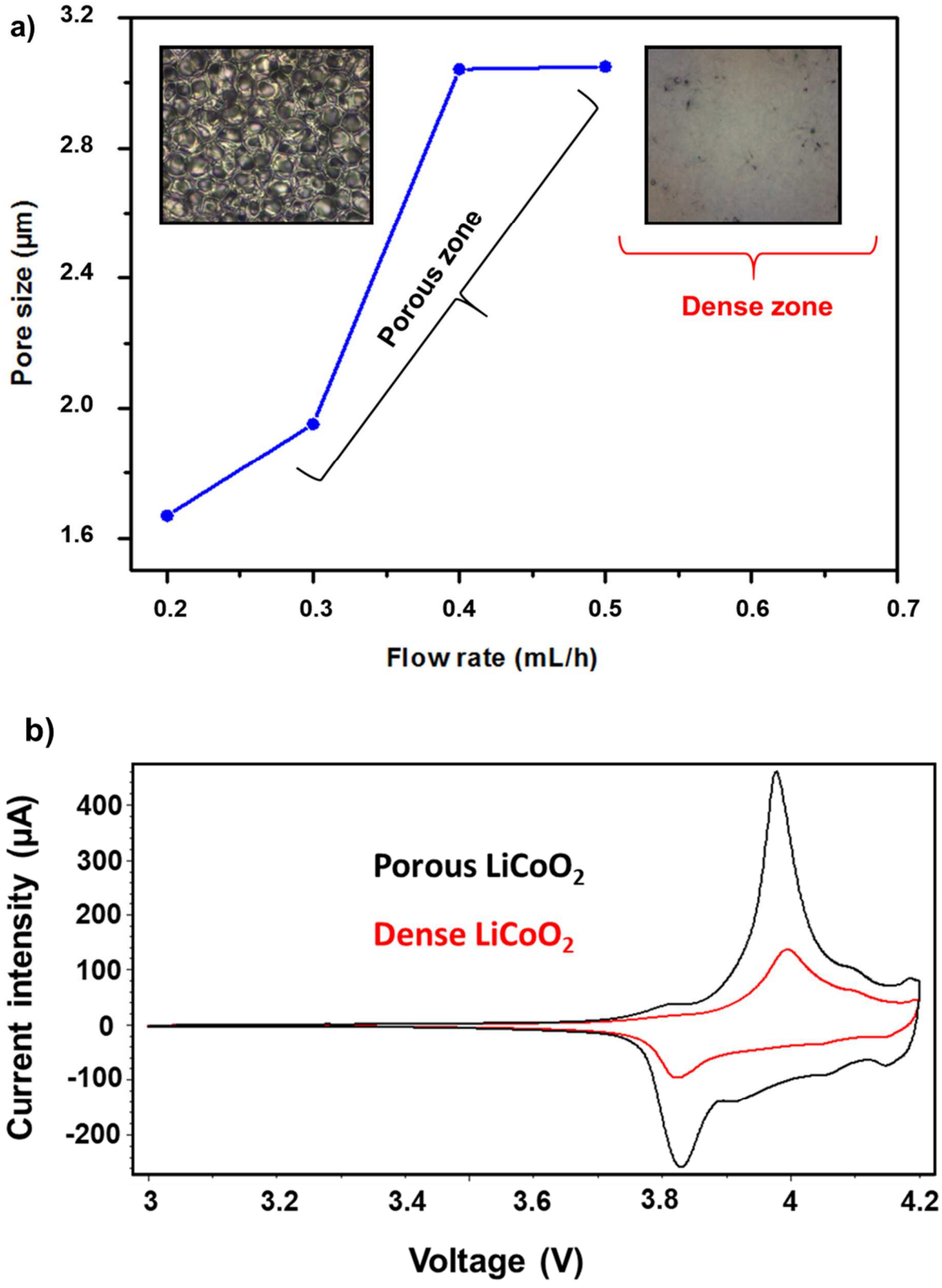

Figure 3: a) The relation between the pore size of $LiCoO_2$ films and the flow rate of the precursor during deposition, b) CV profiles of both films dense and porous.

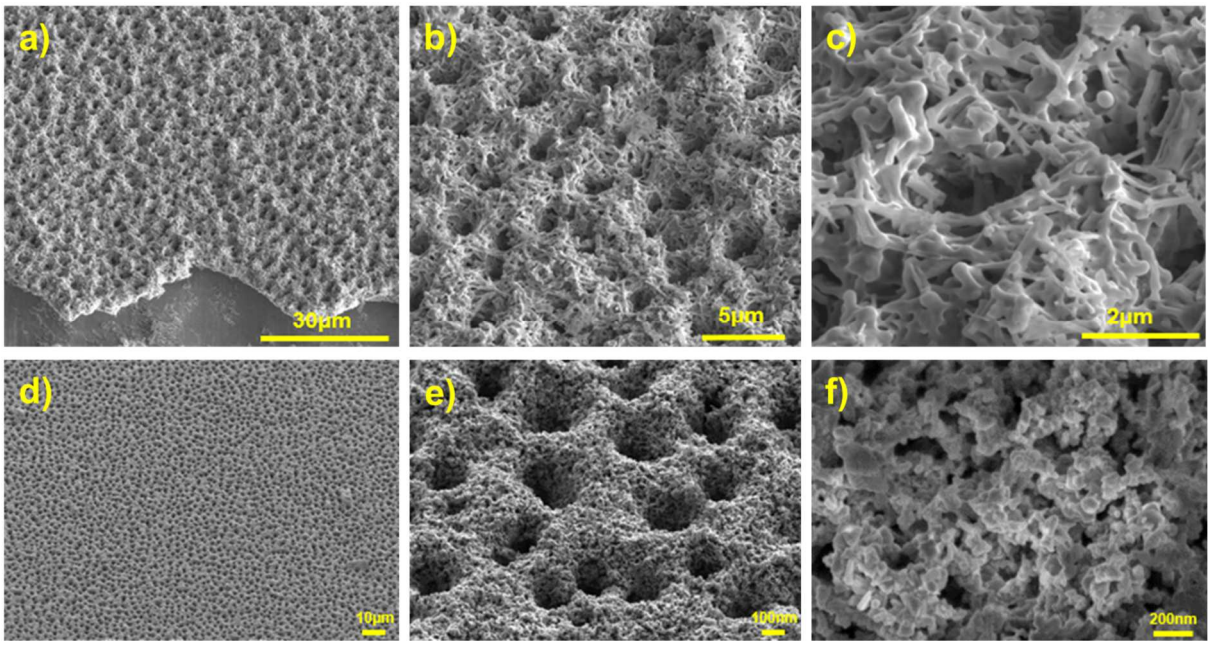

Figure 4: SEM images with different magnifications of porous $LiCoO_2$ layers deposited by electrospray at 250 °C at a flow rate of 0.3 mL/h, (a-c) before annealing and (d-f) after annealing at 600 °C for 2 h.

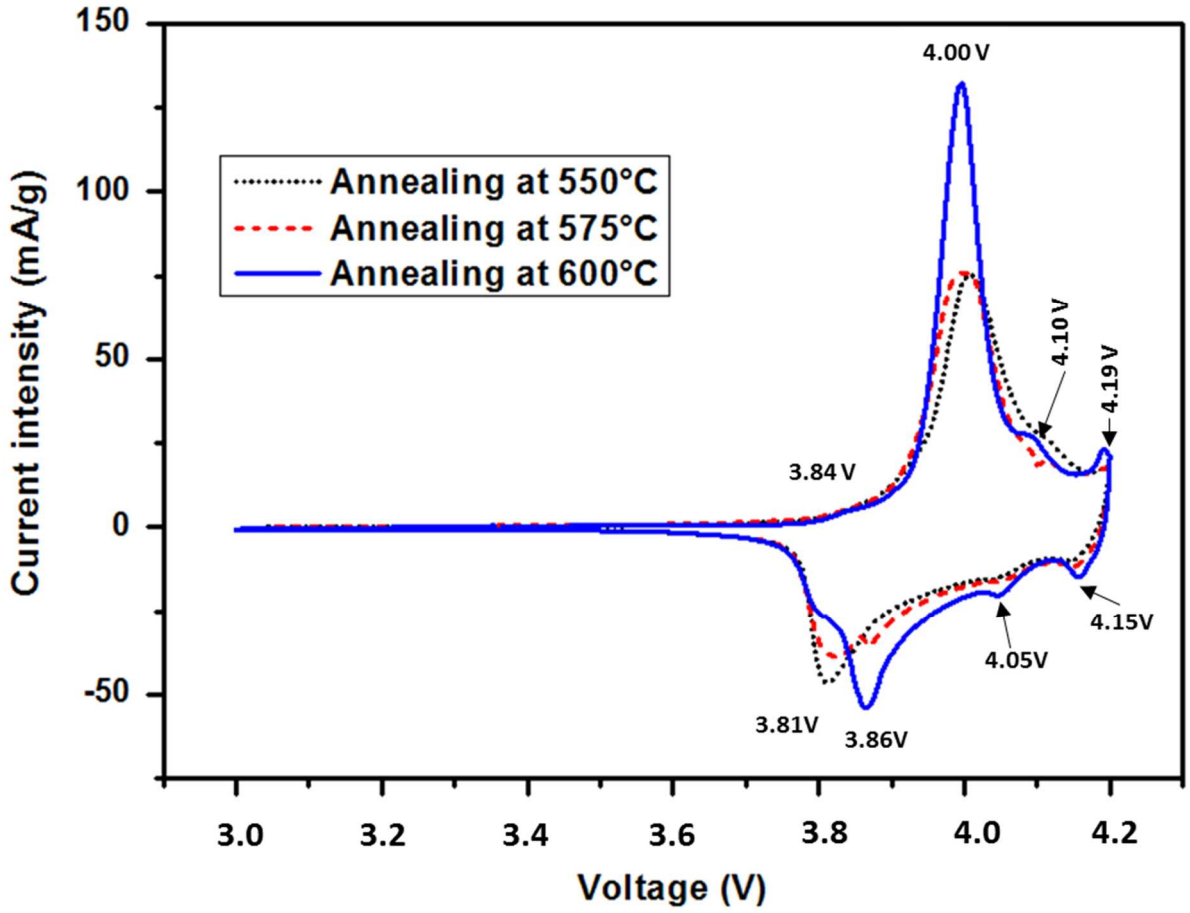

Figure 5: Cyclic voltamogram of a $LiCoO_2$ film cycled between 3 V and 4.2 V with a scan rate 0.05 mV/s at room temperature.

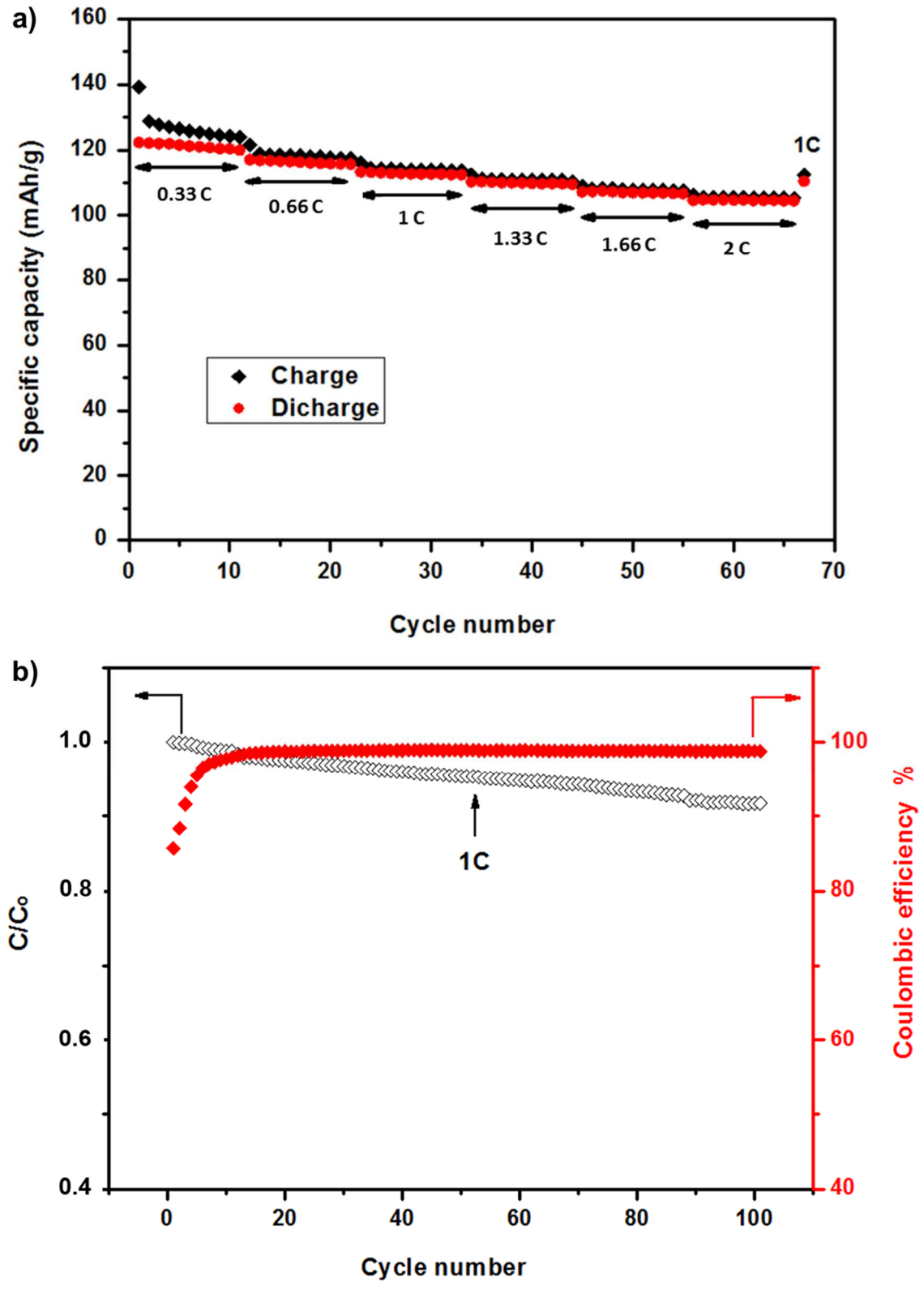

Figure 6: (a) Specific capacity (charge and discharge) of a $LiCoO_2$ film during 68 cycles under various current densities. (b) C/C0 (discharge) and coulombic efficiency of a $LiCoO_2$ film during 100 cycles. The current density is 150 µA/g.

Table 1: Pores diameter at different flow rates

Rate flow (mL/h)	**0.2**	**0.3**	**0.4**	**0.5**	**0.7**
Pore diameter (µm)	1.668	1.951	3.042	3.05	No pores